



Supported gold cluster catalysts prepared by solid grinding using a non-volatile organogold complex for low-temperature CO oxidation and the effect of potassium on gold particle size



Luong Xuan Dien^{a,c}, Tamao Ishida^{a,b,*}, Ayako Taketoshi^{a,b}, Duc Q. Truong^d, Huynh Dang Chinh^c, Tetsuo Honma^e, Toru Murayama^{a,b}, Masatake Haruta^{a,b,*}

^a Research Center for Gold Chemistry, Graduate School of Urban Environmental Sciences, Tokyo Metropolitan University, 1-1 Minami-Osawa, Hachioji, Tokyo 192-0397, Japan

^b Department of Applied Chemistry for Environment, Graduate School of Urban Environmental Sciences, Tokyo Metropolitan University, 1-1 Minami-Osawa, Hachioji, Tokyo 192-0397, Japan

^c School of Chemical Engineering, Hanoi University of Science and Technology, No.1 Dai Co Viet, Hanoi, Viet Nam

^d Ceramics and Biomaterials Research Group, Advanced Institute of Materials Science & Faculty of Applied Sciences, Ton Duc Thang University, Ho Chi Minh City, Viet Nam

^e Japan Synchrotron Radiation Research Institute (JASRI), 1-1-1 Kouto, Sayo, Hyogo 679-5198, Japan

ARTICLE INFO

Keywords:

Gold clusters
Gold catalyst
Solid grinding
CO oxidationion
Air purification

ABSTRACT

We have found that physical mixing (solid grinding, SG) of dimethylgold(III) acetylacetoneate ($\text{Me}_2\text{Au}(\text{acac})$) adsorbed on SiO_2 with potassium *t*-butoxide ($\text{KO}'\text{Bu}$) significantly improved the catalytic activity for CO oxidation at low temperature, and $T_{1/2}$ (the temperature at 50% CO conversion) became extremely low such as -43°C . We have also developed an alternative Au complex for SG, and 2-(*p*-tolyl)pyridinebis(trifluoroacetate) gold(III) (AuTFA) could be adsorbed on metal oxide (MO_x) supports by physical mixing of AuTFA with MO_x in air at room temperature for 20 min, and small Au nanoparticles (NPs) were deposited after calcination. The sizes of Au NPs were almost the same as those prepared using $\text{Me}_2\text{Au}(\text{acac})$ and smaller than those prepared by DP for Al_2O_3 and TiO_2 supports. In addition, grinding AuTFA adsorbed on SiO_2 with $\text{KO}'\text{Bu}$ was also effective for reducing the size of Au particles and gave Au clusters with a mean diameter of 2.2 nm. Moreover, Au/ Al_2O_3 and Au/K- SiO_2 exhibited high catalytic activity for CO oxidation under simulated real exhaust gas conditions (low CO concentration and high humidity up to 100% relative humidity) at ambient temperature.

1. Introduction

Supported gold (Au) catalysts have attracted much attentions over the past three decades because Au exhibits high catalytic activity at low temperatures, e.g., for CO oxidation, and unique catalytic properties [1–5]. To obtain highly active Au catalysts, deposition of Au nanoparticles (NPs) with diameters of less than 5 nm is critically important. Thus, many efforts have been made to develop preparation methods for a wide variety of supports. Deposition-precipitation (DP), in which Au (OH_3) derived from HAuCl_4 is deposited exclusively on metal oxides (MO_x), has been frequently used. [6] However, DP cannot be applied to acidic supports, such as SiO_2 , due to weak interaction between $\text{Au}(\text{OH})_3$ and a negatively charged SiO_2 surface or due to electrostatic repulsion between $\text{Au}(\text{OH})_4^-$ and SiO_2 in neutral or basic conditions.

From this point of view, several methods for deposition of Au NPs and Au clusters with diameters of less than 2 nm onto inert supports including SiO_2 have been developed. These methods include DP using a Au-ethylenediamine complex ($\text{Au}(\text{en})_2\text{Cl}_3$) [7], incipient wetness (IP) using HAuCl_4 followed by ammonia treatment [8], IP using chloride-free Au complexes [9,10], liquid-phase grafting [11,12], gas-phase grafting [13,14], and solid grinding (SG) [15,16]. Among these methods, SG developed by us is a particularly simple method because physical mixing of a volatile organogold complex, such as dimethyl (acetylacetoneate) gold(III) ($\text{Me}_2\text{Au}(\text{acac})$), and supports followed by reduction of Au^{3+} can readily give Au clusters. While gas-phase grafting using $\text{Me}_2\text{Au}(\text{acac})$ should be carried out under reduced pressure (e.g. 1 Pa) to sublime the Au complex and takes long time to gradually deposit the Au complex onto supports, the great advantage of

* Corresponding authors at: Research Center for Gold Chemistry, Graduate School of Urban Environmental Sciences, Tokyo Metropolitan University, 1-1 Minami-Osawa, Hachioji, Tokyo 192-0397, Japan.

E-mail addresses: tamao@tmu.ac.jp (T. Ishida), haruta-masatake@tmu.ac.jp (M. Haruta).

SG is that physical mixing can be carried out under air at room temperature for only 20 min. In addition, SG can be applied to various supports including inert materials such as carbons and polymers [16]. However, the size of Au on SiO_2 prepared by SG is still relatively large (8.4 nm) [15]. In this work, we modified SG and obtained small Au NPs with a mean diameter of 3 nm on SiO_2 . We also report that grinding Au precursor adsorbed SiO_2 with KO°Bu decreased the diameter of Au particles to 2 nm and enhanced the catalytic activity for CO oxidation.

Although $\text{Me}_2\text{Au}(\text{acac})$ is a useful precursor, suppliers are limited due to troublesome synthetic procedures. $\text{Me}_2\text{Au}(\text{acac})$ is synthesized from KAuCl_4 via $[\text{Me}_2\text{Au}]_2$ by Grignard reaction at -42°C to obtain followed by complexation with potassium acetylacetone [17]. Low yield (usually low such as 20%) in the first step and final sublimation at low temperature make difficult to obtain and lead high cost. Thus, $\text{Me}_2\text{Au}(\text{acac})$ is now very expensive; the price is 2880 USD/g from STREM in the U.S. and ca. 11,000 USD/g from Wako Pure Chemical in Japan (searched in August, 2018). This makes $\text{Me}_2\text{Au}(\text{acac})$ difficult to use for practical catalysts in a large scale. In addition, $\text{Me}_2\text{Au}(\text{acac})$ is sensitive to light and air, causing the decomposition and reduction of Au^{3+} to Au^0 during storage. Therefore, development of alternative Au complexes that can be more easily synthesized for SG is highly desired.

In this study, we also aimed development of alternative Au complexes for SG and focused on 2-(*p*-tolyl)pyridinebis(trifluoroacetate) gold(III) (AuTFA) as a new precursor. AuTFA can be synthesized by one step from a commercially available Au complex in excellent yield. We found that AuTFA could be used for SG under the same conditions as the previous study to give Au NPs and Au clusters on SiO_2 , TiO_2 , and Al_2O_3 despite the non-volatility of AuTFA. The mean diameter of Au for Al_2O_3 and TiO_2 obtained by SG using AuTFA was almost comparable to those obtained by SG using $\text{Me}_2\text{Au}(\text{acac})$ and smaller than those prepared by DP except for SiO_2 . The effect of K was much pronounced for AuTFA on SiO_2 and the size of Au could be minimized to about 2 nm.

For application into air purification, catalysts are required to be active under humid air containing low CO concentration. From this point of view, we also report the catalytic activity of Au/MO_x for CO oxidation in air containing 500 ppm CO and H_2O with high concentration.

2. Experimental

2.1. Materials

Gold catalysts, Au/SiO_2 and Au/TiO_2 (1 wt% Au loading), were purchased from Haruta Gold Inc. SiO_2 (Fuji Silysia Chemical LTD., Q-10, 60 μm , specific surface area of $256 \text{ m}^2 \text{ g}^{-1}$), Al_2O_3 (Sumitomo Chemical Co., High Purity Alumina AKP-G015, $148 \text{ m}^2 \text{ g}^{-1}$), and TiO_2 (Titan Kogyo, Ltd., PC-101, $340 \text{ m}^2 \text{ g}^{-1}$) were used as support materials in this study. All of the supports were used as received.

Tetrachloroauric(III) acid tetrahydrate ($\text{H}[\text{AuCl}_4] \cdot 4\text{H}_2\text{O}$), $\text{Au}(\text{OAc})_3$, and $\text{Me}_2\text{Au}(\text{acac})$ were purchased from Kishida Reagents Chemicals Co., Ltd., Alfa Aesar, and Tri Chemical Laboratories Inc., respectively, and were used as gold precursors without further purification.

All reagents 2-(*p*-tolyl)pyridine, trifluoroacetic acid (TFA), potassium *tert*-butoxide (KO°Bu), NaOH, and NaBH_4 and solvents (dichloromethane, hexane, chlorobenzene, acetonitrile, and diethyl ether) were purchased and used without further purifications.

2.2. Synthesis of a gold complex

The complex AuTFA was prepared according to a previously reported method by Tilset et al. with minor modification [18]. A solution of $\text{Au}(\text{OAc})_3$ (0.128 g, 0.34 mmol, 1.00 equiv.) and 2-(*p*-tolyl)pyridine (70 μL , 0.41 mmol, 1.19 equiv.) in a 1:1 mixture of water (5 mL) and TFA (5 mL) was heated in an oil bath at 140°C for 6 h. After the reaction, the light yellow solution was cooled to room temperature, and the supernatant was decanted and was placed into a round-bottom flask.

When the product had been precipitated out, TFA was added to redissolve the product before decantation. Water was added to the flask, and the mixture was cooled to precipitate the product. The precipitate was collected on a fine frit, washed with water and diethyl ether, dried in air at 80°C for 40 min, and finally dried under vacuum at room temperature overnight to obtain AuTFA in 90% yield. An analytical sample was further purified by recrystallization from a mixture of dichloromethane and hexane.

^1H NMR (300 MHz, CD_2Cl_2 , δ in ppm): δ 8.41 (dd, $J = 6.3, 0.9 \text{ Hz}$, 1 H), 8.08 (dt, $J = 7.6, 1.5 \text{ Hz}$, 1 H), 7.76 (dd, $J = 8.3, 1.1 \text{ Hz}$, 1 H), 7.37 (ddd, $J = 7.5, 6.0, 1.4 \text{ Hz}$, 1 H), 7.31 (d, $J = 7.8 \text{ Hz}$, 1 H), 7.16 (ddd, $J = 8.0, 1.4, 0.6 \text{ Hz}$, 1 H), 6.76 (s, 1 H), 2.44 (s, 3 H). ^{13}C NMR (75 MHz, CDCl_3 , δ in ppm): δ 164.9, 147.6, 144.13, 144.07, 142.5, 138.1, 131.0, 129.0, 125.8, 125.6, 124.1, 121.3, 117.4, 22.2. Anal. Calcd. for $\text{C}_{16}\text{H}_{10}\text{AuF}_6\text{NO}_4$: C, 32.51; H, 1.70; N, 2.37. Found: C, 32.44; H, 1.70; N, 2.43.

2.3. Preparation of catalysts

All gold catalysts were prepared with initial loading of 1 wt% Au by three deposition methods: SG, DP, and deposition-reduction (DR). For SG, the support (500 mg) and the Au complex (8.4 mg for $\text{Me}_2\text{Au}(\text{acac})$ or 15.4 mg for AuTFA) were ground in an agate mortar in air at room temperature for 20 min, followed by calcination in air at 300°C for 2 h. The catalysts obtained using $\text{Me}_2\text{Au}(\text{acac})$ and AuTFA were abbreviated as AuAC/MO_x and AuTFA/MO_x , respectively. When KO°Bu was used, after the support (500 mg) and the Au complex (1 wt% Au loading) had been ground for 10 min, KO°Bu (29.3 mg, 2 wt% K loading, and 58.6 mg, 4 wt% K loading for SiO_2) was added to the mixture. Then the mixture was ground further for 10 min, followed by calcination in air at 300°C for 2 h. These catalysts were abbreviated as $\text{AuAC}/\text{K-MO}_x$ and $\text{AuTFA}/\text{K-MO}_x$.

For DP [6], a solution of HAuCl_4 (1.02 mM, 100 mL) was heated to 70°C , and the pH was adjusted to 7 by adding NaOH solution. The support (2 g) was added, and the suspension was stirred at 70°C for 1 h with pH maintained at 7. Then the solid was separated by centrifugation, filtered, washed with water 5 times, and dried at 80°C overnight. The solid was directly subjected to CO oxidation after pretreatment in air at 250°C for 1 h. In another case, the dried solid was calcined in air at 300°C for 4 h.

For DR [19], an appropriate aqueous solution of $\text{Au}(\text{en})_2\text{Cl}_3$ was added to a suspension of SiO_2 (1 g) dispersed in water (200 mL). The pH of the suspension was adjusted to 9 by adding aqueous NaOH solution. The mixture was stirred at room temperature for 30 min, and then an excess amount of an aqueous solution of 0.01 M NaBH_4 was slowly added. After additional stirring at room temperature for 1 h, the mixture was filtered, washed with water 5 times, dried at 120°C overnight, and then calcined in air at 300°C for 4 h.

2.4. Characterization

^1H and ^{13}C NMR spectra were recorded on a JEOL ECS-300 (operating at 300 and 75 MHz, respectively) in CD_2Cl_2 or CDCl_3 (Acros Organics Co., Inc.) with tetramethylsilane (TMS) as an internal standard. The actual gold loadings of the catalyst samples were measured by atomic absorption spectrometry (AAS) using a Shimadzu AA-6200 spectrophotometer. Gold of the catalysts was dissolved into aqua regia, and the solution was filtered and diluted in water to subject it to AAS. Decomposition temperature of AuTFA was measured by thermogravimetric (TG) and differential thermal analyses (DTA) using a Seiko Instruments Inc. (SII) TG/DTA A7200 in a flow of air (200 mL min^{-1}) with heating from room temperature to 800°C at a ramping rate of $10^\circ\text{C min}^{-1}$.

High-angle annular dark-field scanning transmission electron microscopic (HAADF-STEM) observations were carried out using a JEOL JEM-3200FS at 300 kV.

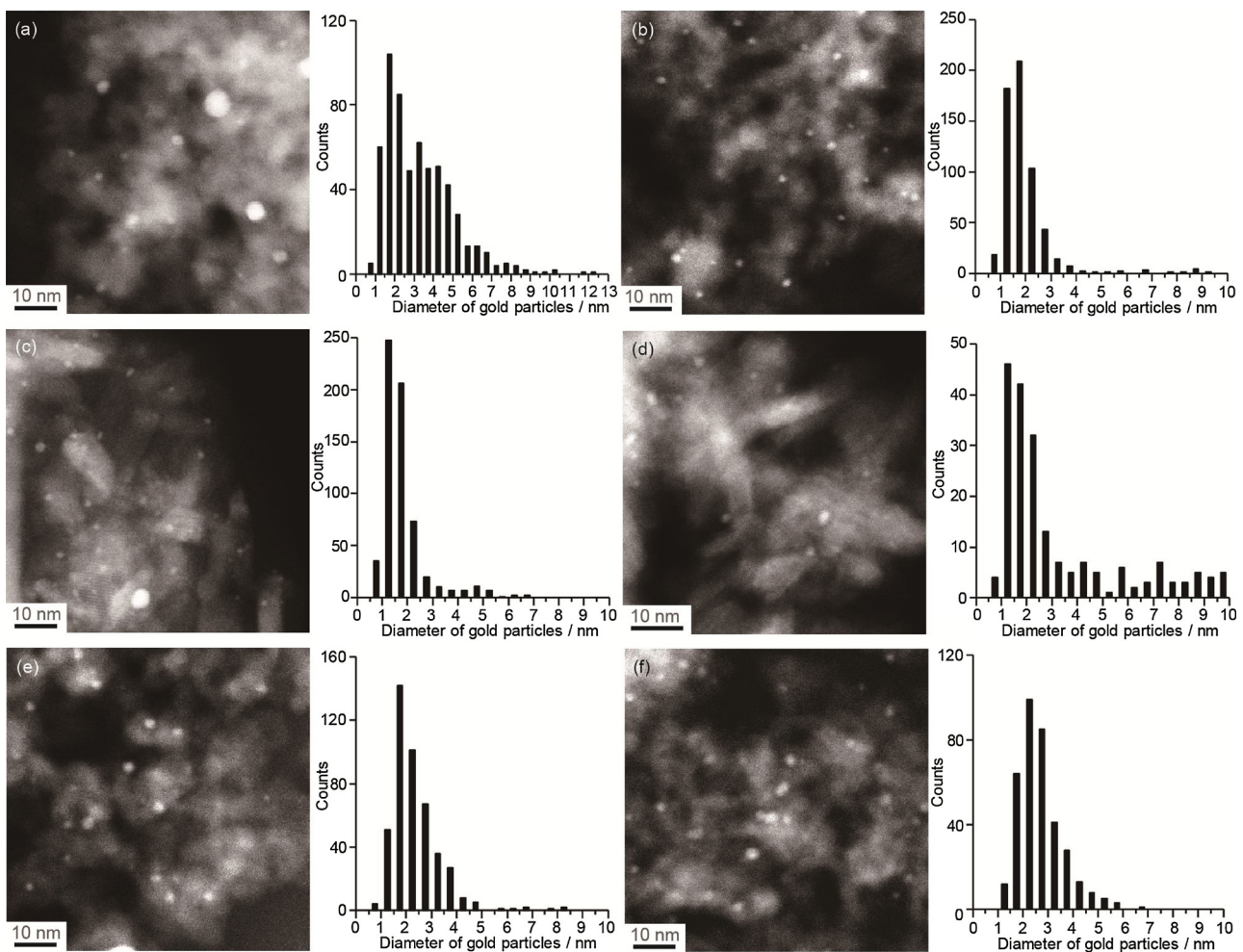


Fig. 1. HAADF-STEM images and size distributions of AuAC/SiO₂ (a), AuAC/K-SiO₂ (b), AuAC/Al₂O₃ (c), AuAC/K-Al₂O₃ (d), AuAC/TiO₂ (e), and AuAC/K-TiO₂ (f).

Au L_{III}-edge X-ray absorption fine structure (XAFS) measurements were carried out at BL14B2 of SPring-8 (Hyogo, Japan). The XAFS samples were ground with boron nitride in an agate mortar and made into pellets. The storage ring energy was 8 GeV with a typical current of 99.5 mA. Au L_{III}-edge (11.92 keV) XAFS spectra were measured using a Si(311) double crystal monochromator in transmission mode. Ionization chambers were used to measure the intensities of the incident and transmitted X-rays, and the quick scan technique (QXAFS) was used in these measurements. Spectral analysis was carried out using the XAFS analysis software programs Athena and Artemis [20]. Estimation of the Au⁰ and Au³⁺ ratio was carried out by linear combination fitting using Au foil and Au(OH)₃ as references for Au⁰ and Au³⁺, respectively. Extraction of the extended X-ray absorption fine structure (EXAFS) oscillation from the spectra, normalization by edge-jump, and Fourier transformation were performed by using Athena. Curve-fitting analysis was carried out in R-space by using Artemis. The *k*-range was 2–12 Å^{−1} and the *r*-range was 1.8–3.2 Å. In the curve-fitting analysis, backscattering amplitude, phase shift, and mean free path of the photoelectrons were calculated by FEFF8.4 [21] and then the other parameters, including the number of neighboring atoms, interatomic distance between the absorbed atom to the neighboring atom, the Debye–Waller factor, and absorption edge energy, were treated as fitting parameters. The intrinsic loss factor was obtained by curve-fitting analysis of the EXAFS data for the Au foil.

Temperature-programmed oxidation (TPO) experiments were carried out using a MicrotracBEL Belcat II equipped with a thermal conductivity detector (TCD) and mass spectrometer (BEL Mass). A sample (200 mg) was treated with 5 vol% O₂ in He (50 mL min^{−1}) at room

temperature for 20 min and heated up to 700 °C with a ramping rate of 5 °C min^{−1}.

Fourier-transformed infrared (FTIR) spectra were recorded on a JASCO, FT/IR-6100 V using the KBr pellet technique in the range of 400 to 4000 cm^{−1}. A background spectrum was collected with 4 cm^{−1} resolution. Diffuse reflectance infrared Fourier transform (DRIFT) spectra were obtained by using JASCO FT/IR-6100 V equipped with a heat chamber (ST Japan, Model – HC500). The sample powder was pretreated in a flow of air (50 mL min^{−1}) at 250 °C for 1 h. Then the sample was exposed to 10 vol% CO in He (40 mL min^{−1}) at −180 °C for 35 min. DRIFT spectra were obtained by subtracting the background spectrum. After Au sites had been saturated with CO, the catalyst was treated in a flow of N₂ (30 mL min^{−1}), and the spectra were collected at −180 °C.

2.5. Catalytic tests

Catalytic tests for CO oxidation were carried out in a fixed-bed glass reactor (internal diameter of 6 mm), containing 0.15 g of a catalyst. Pretreatment was performed in a stream of air at 250 °C for 1 h at a flow rate of 50 mL min^{−1}. After the pretreatment, the catalyst was cooled to room temperature, and the reaction gas (1 vol% CO in air) was passed through the reactor at a flow rate of 50 mL min^{−1} (weight hour space velocity, WHSV = 20,000 mL h^{−1} g_{cat}^{−1}). The outlet gas was analyzed by an on-line gas chromatograph (Ohkura Riken, model 802 or Shimadzu, GC-8 A equipped with Gasukuropack 54 and molecular sieve 13X columns). The production of CO₂ was also measured by the same GC analysis described above. The CO₂ selectivity was almost 100%. The

moisture content in the reaction gas was monitored by a dew point meter (Air Liquid DPO-6), and the water concentrations were in the range of 20–200 ppm. We used $T_{1/2}$, which is the temperature at 50% CO conversion, to discuss catalytic activity.

Kinetic measurements were carried out of different temperatures using 50 mg of the Au catalyst with a support (100 mg). Operation conditions were as follows: WHSV = 20,000 mL h⁻¹ g_{cat}⁻¹, 1 vol% CO in air. The catalysts were pretreated in air (50 mL min⁻¹) at 250 °C for 1 h. The flow rates were changed in the range of 20–100 mL min⁻¹ in order to keep CO conversion below 15%.

CO oxidation under low CO concentration (500 ppm in air) in the presence of water was measured by MicrotracBEL Belcat II equipped with a GC-8 A equipped with a Gasukuropack 54 and molecular sieve 13X column. The catalyst (0.15 g) was charged in a glass cell, and the gas was passed through the catalyst bed. The total flow rate was set to 50 mL min⁻¹. The catalysts were pretreated in air at 250 °C for 1 h.

3. Results and discussion

3.1. Effect of K for AuAC/MO_x

3.1.1. Effect of K on the size of Au particles

We have reported that SG can deposit Au clusters onto inert supports by physical mixing of a volatile Au complex, Me₂Au(acac), and supports followed by a reduction of Au³⁺ [16]. In this work, mixtures of Me₂Au(acac) (1 wt% Au) and MO_x were ground in an agate mortar in air at room temperature and then calcined in air at 300 °C for 2 h to obtain AuAC/MO_x. The actual Au loading was calculated by AAS and exceeded ca. 0.8 wt% for all the catalysts prepared by SG. The sizes of Au particles were estimated by HAADF-STEM (Fig. 1) and these results are summarized in Table 1. According to HAADF-STEM, the mean diameter of Au particles for AuAC/SiO₂ was calculated to be 3.3 ± 1.8 nm (Fig. 1a, Table 1, entry 1), which was smaller than that of Au/SiO₂ (8.4 nm) prepared by SG followed by calcination at 300 °C for 4 h in the previous report by Maeda et al. [15]. Decreased size of Au NPs in this work is probably ascribed to the shorter calcination time; the aggregation of Au NPs during calcination was suppressed.

Grinding Me₂Au(acac) adsorbed on SiO₂ with KO'Bu reduced the size of Au particles when SiO₂ was used as a support, and the size of AuAC/K-SiO₂ was decreased to 2.1 ± 2.1 nm (Fig. 1b, entry 2). Okumura et al. [13] and Scott et al. [14a] have reported that Me₂Au(acac) was physically adsorbed on SiO₂ surface by hydrogen bonding between

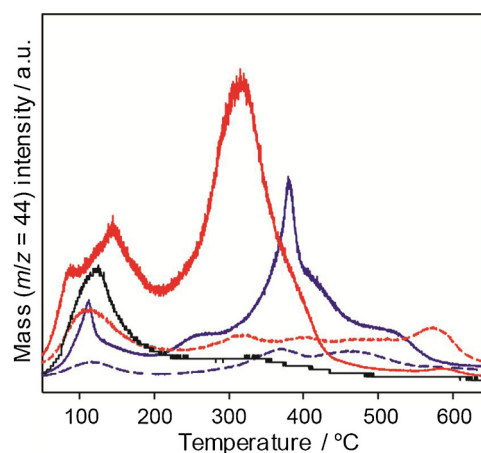


Fig. 2. TPO profiles of AuAC/SiO₂ (blue), AuAC/K-SiO₂ (red), and KO'Bu/SiO₂ (black). Solid and dashed lines indicate before and after calcination at 300 °C for 2 h, respectively.

Si—OH and the oxygen atoms in the acac ligands during gas-phase grafting. Similarly, Me₂Au(acac) was also adsorbed on surface OH groups on SiO₂ during grinding. On the other hand, Gates et al. reported that the acac ligand was removed and ligand exchange occurred with surface OH groups of Al₂O₃ during liquid-phase grafting [12] or by treating in a flow of CO and O₂ [14b]. Physical mixing of KO'Bu with Me₂Au(acac)/SiO₂ might facilitate the ligand exchange. The decomposition behavior of Me₂Au(acac) adsorbed on SiO₂ in the absence or presence of KO'Bu was evaluated by TPO detected by mass spectrometry using *m/z* = 44 (CO₂) peak. CO₂ desorption peaks were observed at 113 and 383 °C for AuAC/SiO₂ before calcination (Fig. 2), which was almost consistent with the previous report by Okumura et al. [13a]. On the other hand, the CO₂ peaks were observed at 91, 140, and 296 °C for AuAC/K-SiO₂ before calcination. Because a CO₂ peak for KO'Bu adsorbed on SiO₂ was observed at 127 °C, the other two peaks were ascribed to the decomposition of Me₂Au(acac) which were shifted to lower temperature than those for AuAC/SiO₂. Therefore, KO'Bu facilitates the decomposition of the Au complex and the reduction to give Au clusters. The effect of K on Au particles size was negligible for Al₂O₃ and TiO₂.

3.1.2. Effect of K on the catalytic activity of AuAC/MO_x

Catalytic activities of AuAC/MO_x were evaluated by CO oxidation. The results are shown in Fig. 3 and Table 1. Generally, Au NPs on inert supports, such as SiO₂, show poor catalytic activity. $T_{1/2}$ of Au/SiO₂ (DR) and Au/SiO₂ (SG) [15] was not observed below 200 °C (Table 1, entries 5 and 6) due to large Au NPs (> 5 nm) and the lack of oxygen vacancy at the Au–SiO₂ interface. However, when the Au particles became small, the catalytic activity was remarkably increased; $T_{1/2}$ of AuAC/SiO₂ was recorded to be 46 °C (entry 1, Fig. 3a). A decrease in CO conversion at temperatures over 150 °C is typically observed in Au on acidic SiO₂ [22] and on polyoxometalate [23].

Grinding Me₂Au(acac)/SiO₂ with KO'Bu significantly improved the catalytic activity, and AuAC/K-SiO₂ exhibited $T_{1/2}$ of –43 °C, which is the highest catalytic activity among the reported Au/SiO₂ catalysts to the best of our knowledge [[7]]. A decrease in $T_{1/2}$ for CO oxidation by Au/SiO₂ from 43 to –10 °C by a post treatment of NaOH aqueous solution was reported by Dai et al., whereas the size of Au NPs increased [7a]. Therefore, the change of surface basicity might also contribute to the enhancement of activity. An effect of K on catalytic activity was also observed for Al₂O₃ and TiO₂ supports. Namely, AuAC/K-Al₂O₃ recorded the same $T_{1/2}$ in spite of larger Au NPs than those for AuAC/Al₂O₃ (Table 1, entries 7 and 8). The catalytic activity of AuAC/K-TiO₂ was also improved compared with that of AuAC/TiO₂ whereas the size of Au was almost the same (Table 1, entries 13 and 14).

Table 1
List of gold catalysts prepared by SG and comparison with previous reports.

Entry	Au catalyst	Method	Au (wt%) ^a	D _{TEM} (nm) ^b	T _{1/2} (°C) ^c
1	AuAC/SiO ₂	SG	0.94	3.3 ± 1.8	46
2	AuAC/K-SiO ₂	SG	0.94	2.1 ± 2.1	–43
3	AuTFA/SiO ₂	SG	0.78	7.3 ± 4.5	> 200
4	AuTFA/K-SiO ₂	SG	0.79	2.2 ± 1.1	91
5	Au/SiO ₂	SG	0.82	8.4	> 200 [15]
6 ^d	Au/SiO ₂	DR	1.07	5.8 ± 2.7	> 200
7	AuAC/Al ₂ O ₃	SG	0.97	1.8 ± 0.9	71
8	AuAC/K-Al ₂ O ₃	SG	0.97	3.6 ± 3.0	71
9	AuTFA/Al ₂ O ₃	SG	0.99	2.4 ± 0.8	141
10	AuTFA/K-Al ₂ O ₃	SG	0.94	3.1 ± 2.7	80
11	Au/Al ₂ O ₃	SG	0.86	2.6 ± 0.8	54 [16b]
12	Au/Al ₂ O ₃	DP	0.98	3.9 ± 3.3	108
13	AuAC/TiO ₂	SG	1.05	2.3 ± 1.0	–1
14	AuAC/K-TiO ₂	SG	1.15	2.7 ± 0.9	–27
15	AuTFA/TiO ₂	SG	0.98	2.3 ± 1.1	1
16	AuTFA/K-TiO ₂	SG	0.99	2.6 ± 0.9	–5
17 ^d	Au/TiO ₂	DP	0.96	4.1 ± 2.2	10

^a Measured by AAS. Initial Au loading was 1.0 wt%.

^b Mean diameter of Au particles was calculated by HAADF-STEM.

^c Temperature at 50% CO conversion for CO oxidation.

^d The catalyst and catalytic data were obtained from Haruta Gold Inc.

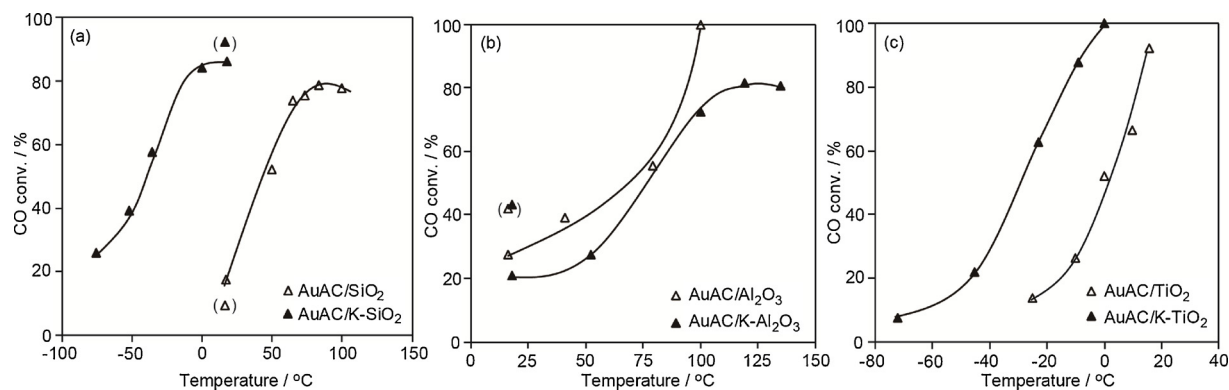


Fig. 3. CO conversion curves as a function of reaction temperature catalyzed by AuAC/SiO₂ (a), AuAC/Al₂O₃ (b), and AuAC/TiO₂ (c) with (▲) or without K (Δ). Conditions: catalyst (150 mg), 1% CO in air (WHSV 20,000 mL h⁻¹ g_{cat}⁻¹). The symbols in parentheses indicate the CO conversions at room temperature obtained after the first run.

3.2. Solid grinding using AuTFA and catalytic activities of AuTFA/MO_x and AuTFA/K-MO_x

3.2.1. Catalyst preparation of Au catalysts using AuTFA with or without K

We also aimed the development of new precursors for SG instead of Me₂Au(acac) and chose AuTFA. According to the literature [13a], Me₂Au(acac) has a flat structure, which enables the adsorption onto MO_x surface without steric hindrance. In the structure of AuTFA, 2-(*p*-tolyl)pyridine ligand has also flat structure, so that AuTFA was expected to be adsorbed on MO_x. AuTFA was synthesized according to the procedure [18] with minor modification in one step from Au(OAc)₃ in excellent yield. AuTFA is stable in light and air and can be stored in air at room temperature for more than a half year, whereas partly reduction of Au³⁺ occurred in Me₂Au(acac) crystal during the storage even under N₂ in a refrigerator. In TG-DTA curves of AuTFA (Fig. S1a), although more than 500 °C is required for complete decomposition, major weight loss is observed in the range of 243–294 °C. Therefore, AuTFA could be used for SG followed by calcination at 300 °C in a similar manner to the previous study [16]. Exothermic DTA peaks were observed at 122, 243, 272, 294, and 524 °C. The first peak at 122 °C with a weight increase was probably due to oxidation. The weight losses at 243–294 and 300–550 °C corresponded to 45% and 22% of the initial weight, being almost consistent with the weights of TFA and 2-(*p*-tolyl)pyridine ligands, respectively. From this result, TFA is removed from AuTFA at first, and then 2-(*p*-tolyl)pyridine moiety is likely to be decomposed and combusted.

According to HAADF-STEM, the mean diameter of Au NPs for AuTFA/SiO₂ was calculated to be 7.3 ± 4.5 nm, which was larger (Fig. 4a, Table 1, entry 3) than that of AuAC/SiO₂ but still smaller than the reported value (8.4 nm, Table 1, entry 5) [15]. SG using AuTFA was effective to deposit small Au NPs onto Al₂O₃ and TiO₂. The mean diameters of Au were estimated to be 2.4 ± 0.8 and 2.3 ± 1.1 nm for AuTFA/Al₂O₃ (Fig. 4c, entry 9) and AuTFA/TiO₂ (Fig. 4e, entry 15), respectively. These values were almost the same as those of AuAC/Al₂O₃ and AuAC/TiO₂, proving that AuTFA is satisfactory as a precursor for SG. It is also noteworthy that SG using AuTFA gave smaller Au NPs than the conventional DP did (Table 1, entries 12 and 17).

In addition, the effect of KOBu was more pronounced for AuTFA than for Me₂Au(acac) when SiO₂ was used as a support. The mean diameter of Au for AuTFA/K-SiO₂ was calculated to be 2.2 ± 1.1 nm (Table 1, entry 4). The effect of KOBu was almost negligible for AuTFA/K-Al₂O₃ (entry 10) and AuTFA/K-TiO₂ (entry 16) in terms of Au particle size as well as AuAC/MO_x. The effect of K will be further discussed below.

Caps et al. used SG for TiO₂ with chloro(triphenylphosphine)gold(I) (Au(PPh₃)Cl) as a precursor, but the obtained Au particles were very large (> 10 nm) probably due to the presence of Cl [24a]. Okumura

also reported SG using Au(PPh₃)Cl to deposit Au NPs on a Na-substituted zeolite, but that complex could not be applied to either SiO₂ or carbons [24b]. In contrast, the use of a chloride-free Au complex in this work successfully gave small Au NPs. Tada et al. have theoretically studied and reported that co-presence of chloride anions with Au atoms and Au clusters accelerated the aggregation of Au because chloride ions were strongly adsorbed on oxygen defect sites of TiO₂ surface [25]. The oxygen defect sites of TiO₂ is also proved to be anchor sites of Au due to the electronic interaction between Au and Ti. Therefore, the presence of Cl⁻ inhibits the stabilizing Au atoms and clusters by TiO₂ surface. In contrast, F atoms of AuTFA is covalently bonded to the carbon atom, so that F atoms in AuTFA could not be directly adsorbed as F⁻ on metal oxide supports. Therefore, halides that do not directly coordinate as F⁻ or present as counter anions in Au complexes do not significantly affect the size of Au particles. Therefore, a flat structure of AuTFA and the structure that halides is not contained as counter ions or directly coordinated would be important factors for suitable Au precursor for SG.

The chemical valence and size of Au particles of AuTFA/K-SiO₂ (Table 1, entry 4) and AuTFA/Al₂O₃ (Table 1, entry 9) were also evaluated by XAFS. According to Au L_{III}-edge X-ray absorption near edge structure (XANES) spectra (Fig. S2a), a cationic Au species was slightly present in AuTFA/K-SiO₂ as judged by the white line peak at 11.92 keV, which is the characteristic peak of cationic Au. The Au⁰/Au³⁺ ratio was estimated to be 95/5 using Au foil and Au(OH)₃ as references. The spectral feature of AuTFA/Al₂O₃ was similar to that of Au foil, suggesting that Au⁰ particles were present as a major species.

Radial structure functions (Fig. S2c) of both catalysts revealed a decrease in the Fourier transformed (FT) magnitude of the peaks at 2.58 and 2.94 Å corresponding to the Au–Au bond length compared with that of Au foil. This result suggested that Au particles became small. Curve-fitting analysis was performed to estimate the mean Au particle size from the coordination numbers (CNs) (Table S1). The mean Au particle sizes were calculated to be 2.0 and 2.6 nm for AuTFA/K-SiO₂ and AuTFA/Al₂O₃, respectively. These values were almost consistent with those estimated by HAADF-STEM. These characterization results suggested that small Au NPs and clusters could be formed by SG using AuTFA.

3.2.2. Catalytic activities of AuTFA/MO_x and AuTFA/K-MO_x

The catalytic activity of AuTFA/MO_x was examined by CO oxidation (Fig. 5). Unfortunately, T_{1/2} of AuTFA/SiO₂ was not observed below 200 °C (Table 1, entry 3) due to the large size of Au NPs. On the other hand, AuTFA/K-SiO₂ significantly improved the catalytic activity and the T_{1/2} was recorded to be 91 °C (Fig. 5a). Grinding AuTFA/SiO₂ with KOBu enables both minimization of Au particle size and improvement the catalytic activity as observed in AuAC/K-SiO₂, although the T_{1/2} of AuTFA/K-SiO₂ was still higher than that of AuAC/K-SiO₂ (entry 2). This

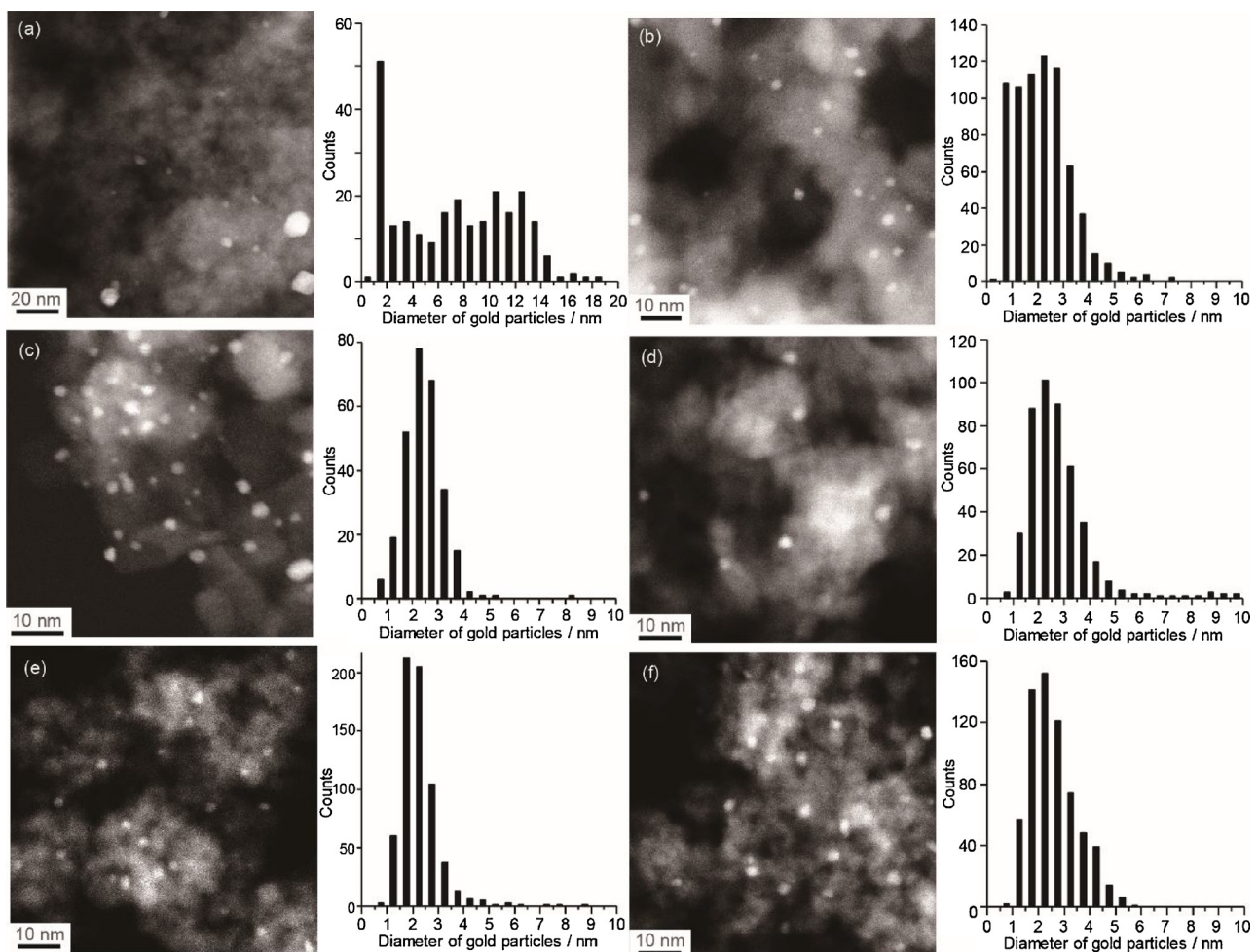


Fig. 4. HAADF-STEM images and size distributions of AuTFA/SiO₂ (a), AuTFA/K-SiO₂ (b), AuTFA/Al₂O₃ (c), AuTFA/K-Al₂O₃ (d), AuTFA/TiO₂ (e), and AuTFA/K-TiO₂ (f).

result indicated that the ligand residue derived from AuTFA still remained partly on the catalyst surface and might block the active sites. However, Au on inert SiO₂ generally shows low catalytic activity ($T_{1/2} > 200$ °C) for CO oxidation, and Au/SiO₂-catalyzed CO oxidation at room temperature is generally achieved by higher loading of Au exceeding 6 wt% [13b,22]. Therefore, it can be said that the $T_{1/2}$ (91 °C) of 1 wt% AuTFA/K-SiO₂ is much improved compared with the conventional Au/SiO₂ catalysts. Interestingly, CO conversion significantly increased when the catalyst was cooled to room temperature after the

first run, particularly for AuTFA/K-SiO₂ (Fig. 5a) and AuTFA/K-Al₂O₃ (Fig. 5b). Although the phenomenon is not clear at this stage, it is noteworthy that $T_{1/2}$ of AuTFA/K-SiO₂ reached room temperature after the first run.

The effect of K on catalytic activity was also observed for Al₂O₃ and TiO₂ supports. Namely, AuTFA/K-Al₂O₃ (entry 10) recorded much higher CO conversion (80 °C) than AuTFA/Al₂O₃ did (entry 9, 141 °C), whereas larger Au particles were deposited on K-Al₂O₃. AuTFA/K-TiO₂ also showed a similar tendency.

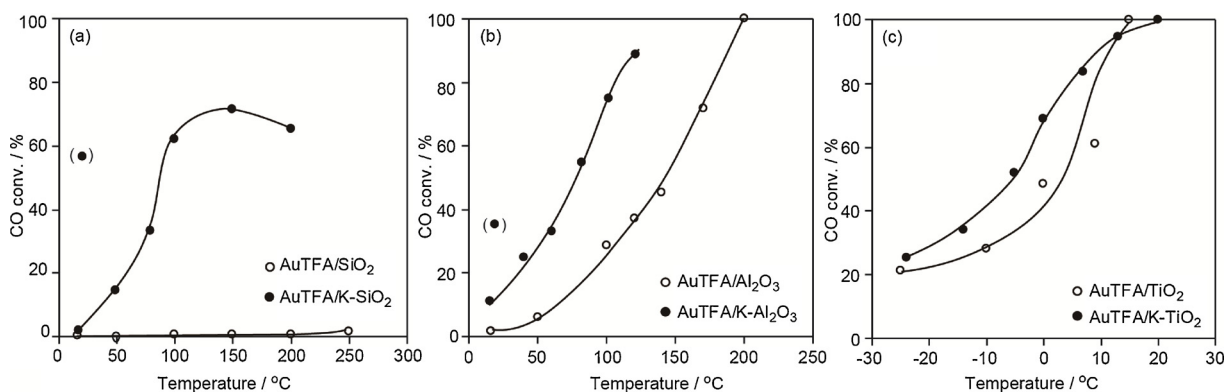


Fig. 5. CO conversion curves as a function of reaction temperature catalyzed by AuTFA/SiO₂ (a), AuTFA/Al₂O₃ (b), and AuTFA/TiO₂ (c) with or without K. Conditions: catalyst (150 mg), 1% CO in air (WHSV 20,000 mL h⁻¹ g_{cat}⁻¹). The symbols in parentheses indicate the CO conversions at room temperature obtained after the first run.

Deposition of alkali metals, particularly K, has been commonly used for tuning catalytic activity and selectivity of metal catalysts [26,27]. The presence of K generally affects the electronic interaction between metal NPs and MO_x supports, reducibility of metal precursors, sintering of metal NPs during thermal treatment, and MO_x surface modification but rarely changes the size of metal NPs. The reduction temperature of Pd^{2+} was increased by K doping, which was ascribed to a strong interaction between K^+ and Pd^{2+} and formation of a mixed KPdO [27]. The opposite phenomenon, i.e., the decrease in the decomposition temperature of AuTFA was observed in this work. Previous studies reported the electron transfer from supports to Pd [27b,c]. The XAFS results revealed the presence of a cationic Au species in AuTFA/K-SiO₂ but its absence in AuTFA/Al₂O₃ despite similar Au particle sizes. The presence of cationic Au species on K-MO_x was also proved by DRIFT spectra (Fig. S4 and Table S2). Therefore, electronic transfer from K to Au is not likely for AuTFA/K-SiO₂. It is known that cationic Au species are present at the perimeter interface, which is known as the active sites for CO oxidation. The increased $\text{Au}^{\delta+}$ fraction suggests the decrease in the size. One of our authors [6c,28] and Lu et al. [29] reported that the amount of cationic Au species did not directly correlate with the catalytic activity for CO oxidation. Therefore, the electronic interaction between K and Au is not the major reason for the improved activity. As mentioned above, Dai et al. [7] reported that the treatment of Au/SiO₂ with NaOH improved the catalytic activity. Therefore, the change of surface basicity would directly correlate to the CO oxidation, although the mechanism in detail is still not clear.

3.3. Characterization of AuTFA/MO_x and AuTFA/K-MO_x

It has been revealed that AuTFA can be used as an alternative precursor for SG; the size of Au NPs on Al₂O₃ and TiO₂ were almost same as those obtained using Me₂Au(acac) characterized by HAADF-STEM and XAFS in spite of non-volatility of AuTFA. The catalytic activities of AuTFA/Al₂O₃ and AuTFA/TiO₂ with or without K altered corresponding to the size of Au particles and were comparable to those of AuAC/Al₂O₃ and AuAC/TiO₂ with or without K, respectively. Although the size of Au NPs of AuTFA/SiO₂ was larger than AuAC/SiO₂, the particle size could be minimized to 2.2 nm by grinding with KO'Bu. In addition, the activity of AuTFA/K-SiO₂ was significantly improved from the conventional Au/SiO₂. In this section, we further studied the decomposition behavior of AuTFA on MO_x supports and the effect of K during the catalyst preparation.

3.3.1. FT-IR

The decomposition of AuTFA on MO_x was also confirmed by FTIR spectra (Fig. S3). Characteristic absorption peaks of AuTFA were observed at 1437, 1467, and 1498 cm⁻¹ in the region of C=C and C=N ring stretch vibrations. These peaks were also clearly observed after grinding AuTFA, MO_x, and/or KO'Bu but had almost disappeared after calcination in air at 300 °C for 2 h.

3.3.2. TPO

Thermal decomposition behavior of AuTFA/MO_x and AuTFA/K-MO_x was examined by TPO (Fig. 6). In the case of AuTFA/SiO₂ before calcination (Fig. 6a, blue solid line), CO₂ peaks were observed at 252, 415, and 542 °C, which were in agreement with the TG-DTA profile of AuTFA (Fig. S1a). After calcination at 300 °C, the peak at 252 °C disappeared (blue dashed line), but the latter two CO₂ peaks were still observed. Although the ligand residue was not detected by FTIR, the ligand still remained to some extent on the catalyst surface according to TPO.

CO₂ peaks of AuTFA/Al₂O₃ (Fig. 6b, blue solid lines) before calcination were observed at 393 and 466 °C, which were shifted to a lower temperature compared with those of AuTFA/SiO₂ (Fig. 6a). The shift in lower temperature was also observed in AuTFA/TiO₂ at 301, 329, and 367 °C (Fig. 6c, blue solid lines). These results indicated that the

interaction between AuTFA and MO_x supports affects the decomposition behavior of AuTFA. After the calcination, the peak area of AuTFA/Al₂O₃ and AuTFA/TiO₂ significantly decreased (blue dashed line), while the ligand residue was hardly removed from the AuTFA/SiO₂. Given that AuTFA/Al₂O₃ and AuTFA/TiO₂ gave smaller Au NPs than AuTFA/SiO₂ did, the decomposition of AuTFA on Al₂O₃ and TiO₂ was facilitated at lower temperatures, and this might be the reason for small Au NPs being obtained without KO'Bu.

The decomposition temperatures altered for not only AuTFA but also KO'Bu. Namely, KO'Bu on SiO₂ was easily decomposed at around 130 °C (Fig. 6a, black line), while the decomposition temperature of KO'Bu was 258 °C by TG-DTA (Fig. S1b) and ranged from 50 to 400 °C on TiO₂ (Fig. 6c, black line). These results suggest that neutralization of acidic SiO₂ promoted decomposition of the *t*-butoxy group. When AuTFA/SiO₂ and KO'Bu were ground, CO₂ peaks were significantly shifted to lower temperatures at 105, 208, and 325 °C (Fig. 6a, red solid line). From the results for KO'Bu on SiO₂, the latter two peaks were ascribed to the decomposition of AuTFA. The remarkable decrease in decomposition temperature suggests that KO'Bu promotes both of the decomposition of AuTFA and the subsequent reduction of Au^{3+} at a low temperature, resulting in small Au particles. After air calcination at 300 °C for 2 h, the ligand was almost completely removed from the catalyst surface, and CO₂ peaks markedly decreased (Fig. 6a, red dashed line).

As well as Me₂Au(acac), AuTFA would also be weakly adsorbed by hydrogen bonds between oxygen atoms in trifluoroacetate moieties and surface hydroxy groups on pristine SiO₂, and KO'Bu would accelerate the ligand exchange of AuTFA. The adsorbed residual 2-(*p*-tolyl)pyridinegold(III) species might be decomposed at a lower temperature than AuTFA itself.

With regard to AuTFA/K-Al₂O₃ before calcination, the CO₂ peaks were also shifted to lower temperatures at 143, 222, 340, and 402 °C (Fig. 6b, red solid line) than those for AuTFA/Al₂O₃, but the decrease in temperature was less pronounced compared with that for AuTFA/K-SiO₂. The decomposition temperature of AuTFA/K-TiO₂ before calcination did not change from that of AuTFA/TiO₂ (Fig. 6c, red solid line). Therefore, the effect of K on the Au particle size were not remarkable on Al₂O₃ and TiO₂.

3.4. Kinetic studies and application for CO oxidation using simulated real exhaust gas

Initially, the catalyst durability was examined (Fig. S6). AuTFA/K-SiO₂, AuTFA/TiO₂, and AuTFA/Al₂O₃ showed excellent stability for CO oxidation. AuTFA/TiO₂ maintained its catalytic activity at full CO conversion for 17 h at 25 °C. AuTFA/K-SiO₂, AuTFA/Al₂O₃, and AuAC/K-SiO₂ also maintained their activity at constant CO conversion for more than 15 h. No obvious deactivation was observed for any of the Au catalysts.

3.4.1. Arrhenius plots

The apparent activation energies (E_a) for CO oxidation were calculated by Arrhenius plots (Fig. 7) and were 39.5, 21.9, 32.5, and 26.6 kJ mol⁻¹ for AuTFA/K-SiO₂, AuTFA/Al₂O₃, AuTFA/TiO₂, and AuAC/K-SiO₂, respectively. They are in the range of the reported values, indicating that the reaction mechanism is similar to that previously reported [1,3].

3.4.2. CO oxidation under low CO concentration in the presence of water

Recently, many researchers have focused on a promotion effect of water on Au-catalyzed CO oxidation. It has been revealed that moisture in the reactant gas increased the reaction rates, and reaction mechanisms of CO oxidation involving H₂O have been also discussed [22,23,30–33]. One of our authors reported that the reaction rates of CO over Au/Al₂O₃ and Au/SiO₂ were enhanced with increasing water concentration up to 0.6 vol% [22]. For application into air purification,

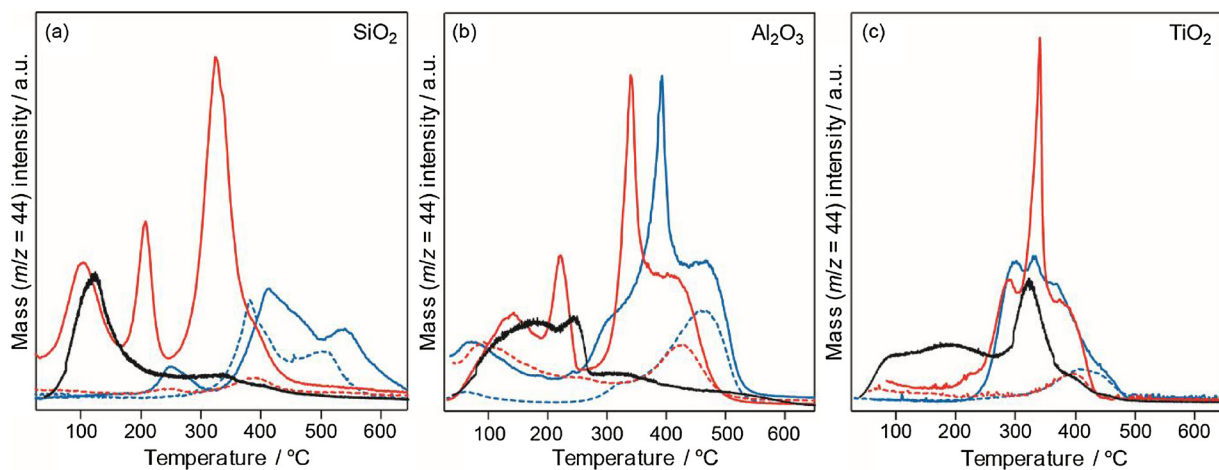


Fig. 6. TPO profiles of AuTFA/SiO₂ (a), AuTFA/Al₂O₃ (b), and AuTFA/TiO₂ (c) with or without KO^tBu. Blue: AuTFA/MO_x, red: AuTFA/K-MO_x, black: KO^tBu on MO_x prepared by grinding at room temperature for 20 min. Solid and dashed lines indicate before and after air calcination at 300 °C for 2 h, respectively.

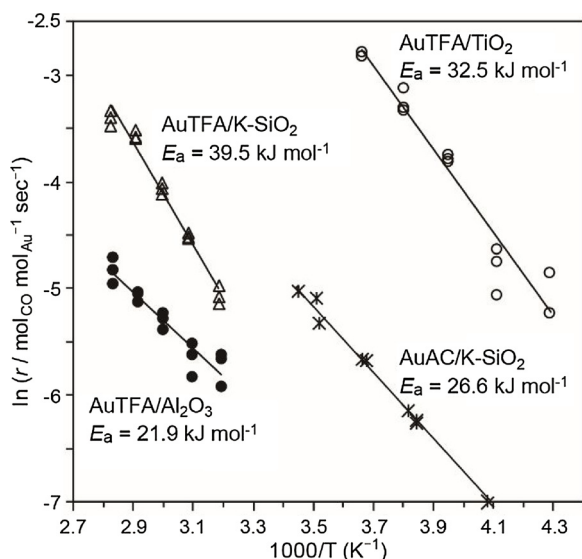


Fig. 7. Arrhenius plots and activation energies (*E_a*) of AuTFA/K-SiO₂ (Δ), AuTFA/Al₂O₃ (\bullet), AuTFA/TiO₂ (\circ), and AuAC/K-SiO₂ (\times). Conditions: a mixture of a Au catalyst (50 mg) and a support (100 mg), 1 vol% CO in air with change in the flow rate. For AuAC/K-SiO₂, 30 mg of Au catalyst was used. The catalysts were pretreated in air (50 mL min⁻¹) at 250 °C for 1 h.

high catalytic activity in humid air containing much higher water concentration at relatively low temperature is demanded. However, high catalytic activity under high water concentration has rarely been reported except for Au/BN using 1 vol% CO in humid air [30] due to the fact that water molecules block the active sites. In addition, CO oxidation catalysts under low CO concentration, such as ppm level, are also desired for purification of real exhaust gas. To get insight of the Au catalysts for application into air purification, AuAC/K-SiO₂, AuTFA/K-SiO₂, AuTFA/Al₂O₃, and AuTFA/TiO₂ were tested for CO oxidation under simulated real exhaust conditions including CO (500 ppm) and water (1–4 vol%) in air at 30 °C.

As shown in Fig. 8, AuTFA/TiO₂ completely converted CO to CO₂ under low CO concentration, but the catalytic activity decreased when water vapour (even 1 vol%) was added. In contrast, the catalytic activity of AuTFA/Al₂O₃ was maintained in humid air even containing 4 vol% H₂O that almost equals to 100% relative humidity (RH). Furthermore, the catalytic activity of AuTFA/K-SiO₂ in humid air increased compared with dry conditions, and the CO conversion was recorded to be 60% under 100% RH at 30 °C. SiO₂ had not been regarded as a

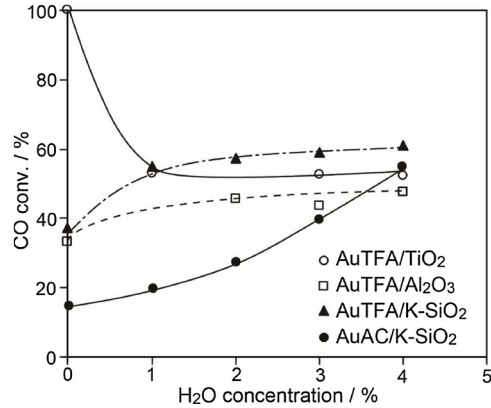


Fig. 8. CO conversion over AuTFA/TiO₂ (○), AuTFA/Al₂O₃ (□), and AuTFA/K-SiO₂ (▲), and AuAC/K-SiO₂ (●) at 30 °C. as a function of H₂O concentration. Conditions: catalyst (30 mg for AuAC/K-SiO₂ and 150 mg for other catalysts), 500 ppm CO in air, 30 °C. H₂O vapour was added, and the total gas flow was set to 50 mL min⁻¹. The catalysts were pretreated in air (50 mL min⁻¹) at 250 °C for 1 h.

suitable support for Au because small Au clusters could not be deposited by conventional methods, resulting in poor catalytic activity for CO oxidation. It is noteworthy that AuTFA/K-SiO₂ can be easily prepared and catalyze CO oxidation at ambient temperature in humid air. AuAC/K-SiO₂ recorded full conversions regardless of the water concentration. When a decreased amount (30 mg) of AuAC/K-SiO₂ was used, a positive effect of water concentration was also observed as well as AuTFA/K-SiO₂ and AuTFA/Al₂O₃. These results suggest that Au/SiO₂ prepared by SG is a promising candidate for application into air purification.

4. Conclusions

In this work, we successfully deposited Au clusters and small Au NPs on metal oxides by SG using Me₂Au(acac) and AuTFA. Grinding the Au complex/MO_x with KO^tBu improved the catalytic activity for CO oxidation remarkably. In particular, AuAC/K-SiO₂ exhibited extremely high catalytic activity at low temperature; the T_{1/2} was –43 °C which is the lowest value for Au/SiO₂ to the best of our knowledge.

Although Me₂Au(acac) is useful precursor for SG, its extremely high cost limits Au catalyst to practical applications. Therefore, we explored an alternative Au precursor, AuTFA, for SG. AuTFA was easily synthesized from commercially available Au(OAc)₃ in one step in excellent yield. AuTFA was stable in light and air, and can be stored in air at room temperature without any changes. AuTFA appeared to be an

efficient precursor for SG even though it has high thermal stability and non-volatility. The sizes of Au particles for AuTFA/Al₂O₃ and AuTFA/TiO₂ were almost comparable to those prepared using Me₂Au(acac) and smaller than those prepared by DP. The effect of KO'Bu was more pronounced for AuTFA with SiO₂. Accordingly, the mean diameter of Au NPs significantly decreased from 7.3 nm (AuTFA/SiO₂) to 2.2 nm (AuTFA/K-SiO₂). KO'Bu would accelerate the ligand exchange between AuTFA and surface OH groups of SiO₂, according to TPO, KO'Bu facilitated the decomposition of AuTFA at lower temperature especially on SiO₂. KO'Bu not only influences the size of Au but also modifies the surface basicity of supports, significantly improving the catalytic activity for CO oxidation. Whereas T_{1/2} of AuTFA/SiO₂ was not observed below 200 °C, T_{1/2} of AuTFA/K-SiO₂ was surprisingly decreased to 91 °C. Since SG using AuTFA is applicable to all kinds of supports including SiO₂ and is easily performed under air at room temperature without the production of waste water, we expect that this method will become a versatile method for preparing various kinds of practical Au catalysts. The obtained catalysts showed high catalytic performance for CO oxidation at ambient temperature even low CO concentration. Water accelerated the CO oxidation for AuTFA/Al₂O₃, AuTFA/K-SiO₂, and AuAC/K-SiO₂ and their catalytic activities were maintained even in 100% RH humid air. These catalysts will be highly advantageous for purification of real exhaust gas.

Declaration of interest

None.

Acknowledgements

This work was financially supported by a Grant-in-Aid for Scientific Research (C) (No. 16K06858) from MEXT, Japan, and a National Foundation for Science & Technology Development (NAFOSTED) grant funded by the Vietnamese Ministry of Science and Technology (Grant No. 104.05-2017.26). L. X. D. is grateful to Tokyo Metropolitan University (TMU) for pre-doctoral and postdoctoral fellowships. The synchrotron radiation experiments were performed at the BL14B2 in SPring-8, Japan, with the approval of JASRI (No. 2016A1521). We appreciate Mr. T. Sakurai for elemental analyses and Mr. E. Watanabe for helping with HAADF-STEM observations at TMU.

Appendix A. Supplementary data

Supplementary material related to this article can be found, in the online version, at doi:<https://doi.org/10.1016/j.apcatb.2018.09.053>.

References

- [1] (a) T. Ishida, H. Koga, M. Okumura, M. Haruta, Chem. Rec. 16 (2016) 2278–2293;
- (b) M. Okumura, T. Fujitani, J. Huang, T. Ishida, ACS Catal. 5 (2015) 4699–4707.
- [2] G.C. Bond, C. Louis, D.T. Thompson (Eds.), *Catalysis by Gold*, Imperial College Press, London, 2006.
- [3] T. Takei, T. Akita, I. Nakamura, T. Fujitani, M. Okumura, K. Okazaki, J. Huang, T. Ishida, M. Haruta (Eds.), *Advances in Catalysis*, 55, 2012, pp. 1–247.
- [4] A. Corma, H. Garcia, Chem. Soc. Rev. 37 (2008) 2096–2126.
- [5] A. Corma, A. Leyva-Pérez, M.J. Sabater, Chem. Rev. 111 (2011) 1657–1712.
- [6] (a) M. Haruta, S. Tsubota, T. Kobayashi, H. Kageyama, M.J. Genet, B. Delmon, J. Catal. 144 (1993) 175–192;
- (b) C. Qi, J. Huang, S. Bao, H. Su, T. Akita, M. Haruta, J. Catal. 281 (2011) 12–20;
- (c) A. Taketoshi, T. Ishida, H. Ohashi, T. Honma, M. Haruta, Chin. J. Catal. 38 (2017) 1888–1898;
- (d) M. Ikegami, T. Matsumoto, Y. Kobayashi, Y. Jikihara, T. Nakayama, H. Ohashi, T. Honma, T. Takei, M. Haruta, Appl. Catal. B: Environ. 134 (135) (2013) 130–135;
- (e) X. Feng, X. Duan, G. Qian, X. Zhou, D. Chen, W. Yuan, Appl. Catal. B: Environ. 150 (151) (2014) 396–401;
- (f) X. Liu, B. Hu, K. Fujimoto, M. Haruta, M. Tokunaga, Appl. Catal. B: Environ. 92 (2009) 411–421.
- [7] (a) H. Zhu, Z. Ma, J.C. Clark, Z. Pan, S.H. Overbury, S. Dai, Appl. Catal. A Gen. 326 (2007) 89–99;
- (b) H. Zhu, C. Liang, W. Yan, S.H. Overbury, S. Dai, J. Phys. Chem. B 110 (2006) 10842–10848;
- (c) Z. Ma, S. Dai, ACS Catal. 1 (2011) 805–818.
- [8] L. Delannoy, N.E. Hassan, A. Musi, N.N.L. To, J.-M. Krafft, C. Louis, J. Phys. Chem. B 110 (2006) 22471–22478.
- [9] H. Sakurai, K. Koga, Y. Iizuka, M. Kiuchi, Appl. Catal. A Gen. 462 (463) (2013) 236–246.
- [10] H. Murayama, T. Hasegawa, Y. Yamamoto, M. Tone, M. Kimura, T. Ishida, T. Honma, M. Okumura, A. Isogai, T. Fujii, M. Tokunaga, J. Catal. 353 (2017) 74–80.
- [11] (a) D. Gajan, K. Guillois, P. Delichére, J.-M. Basset, J.-P. Candy, V. Caps, C. Copréat, A. Lesage, L. Emsley, J. Am. Chem. Soc. 131 (2009) 14667–14669;
- (b) G. Siddiqi, V. Mougel, C. Copréat, Dalton Trans. 44 (2015) 14349–14353.
- [12] J. Guzman, B.C. Gates, Langmuir 19 (2003) 3897–3903.
- [13] (a) M. Okumura, S. Tsubota, M. Haruta, J. Mol. Catal. A Chem. 199 (2003) 73–84;
- (b) M. Okumura, S. Nakamura, S. Tsubota, T. Nakamura, M. Azuma, M. Haruta, Catal. Lett. 51 (1998) 53–58.
- [14] (a) M. Hisamoto, R.C. Nelson, M.-Y. Lee, J. Eckert, S.L. Scott, J. Phys. Chem. C 113 (2009) 8794–8805;
- (b) J.C. Fierro-Gonzalez, B.C. Gates, Langmuir 21 (2005) 5693;
- (c) J. Lu, C. Aydin, N.D. Browning, B.C. Gates, Angew. Chem. Int. Ed. 51 (2012) 5842–5846.
- [15] Y. Maeda, T. Akita, M. Kohyama, Catal. Lett. 144 (2014) 2086–2090.
- [16] (a) T. Ishida, M. Nagaoaka, T. Akita, M. Haruta, Chem. Eur. J. 14 (2008) 8456–8460;
- (b) T. Ishida, N. Kinoshita, H. Okatsu, T. Akita, T. Takei, M. Haruta, Angew. Chem. Int. Ed. 47 (2008) 9265–9268;
- (c) T. Ishida, N. Kawakita, T. Akita, M. Haruta, Gold Bull. 42 (2009) 267–274;
- (d) H. Okatsu, N. Kinoshita, T. Akita, T. Ishida, M. Haruta, Appl. Catal. A Gen. 369 (2009) 8–14;
- (e) T. Ishida, H. Watanabe, T. Bebeko, T. Akita, M. Haruta, Appl. Catal. A Gen. 377 (2010) 42–46;
- (f) J. Huang, T. Akita, J. Faye, T. Fujita, T. Takei, M. Haruta, Angew. Chem. Int. Ed. 48 (2009) 7862–7866;
- (g) J. Huang, T. Takei, T. Akita, H. Ohashi, M. Haruta, Appl. Catal. B: Environ. 95 (2010) 430–438.
- [17] G.I. Zharkova, I.A. Baidina, I.K. Igumenov, J. Struct. Chem. 47 (2006) 1117–1126.
- [18] (a) E. Langseth, C.H. Görbitz, R.H. Heyn, M. Tilset, Organometallics 31 (2012) 6567–6571;
- (b) M.S.M. Holmsen, A. Nova, D. Balcells, E. Langseth, S.Ø. Ødegaard, E.A. Træseth, R.H. Heyn, M. Tilset, Dalton Trans. 45 (2016) 14719–14724.
- [19] T. Ishida, K. Kuroda, N. Kinoshita, W. Minagawa, M. Haruta, J. Colloid Interface Sci. 323 (2008) 105–111.
- [20] B. Ravel, M. Newville, J. Synchrotron Radiat. 12 (2005) 537–541.
- [21] A.L. Ankudinov, A.I. Nesvizhskii, J.J. Rehr, Phys. Rev. B 67 (2003) 115120.
- [22] M. Daté, M. Okumura, S. Tsubota, M. Haruta, Angew. Chem. Int. Ed. 43 (2004) 2129–2132.
- [23] T. Yoshida, T. Murayama, N. Sakaguchi, M. Okumura, T. Ishida, M. Haruta, Angew. Chem. Int. Ed. 57 (2018) 1523–1527.
- [24] (a) C. Marchal, A. Piquet, M. Behr, T. Cottineau, V. Papaefthimiou, V. Keller, V. Caps, J. Catal. 352 (2017) 22–34;
- (b) K. Okumura, Synlett 27 (2016) 1223–1226.
- [25] (a) K. Tada, K. Sakata, S. Yamada, K. Okazaki, Y. Kitagawa, T. Kawakami, S. Yamanaka, M. Okumura, Mol. Phys. 112 (2014) 385–392;
- (b) K. Tada, H. Koga, A. Hayashi, Y. Kondo, T. Kawakami, S. Yamanaka, M. Okumura, Bull. Chem. Soc. Jpn. 90 (2017) 506–519.
- [26] J. Huang, T. Takei, H. Ohashi, M. Haruta, Appl. Catal. A Gen. 435 (436) (2012) 115–122.
- [27] (a) P. Pallegri, G. Leofanti, G. Agostini, L. Bertinetti, S. Bertarione, E. Groppo, A. Zecchina, C. Lamberti, J. Catal. 267 (2009) 40–49;
- (b) W. Zhang, Y. Zhu, S. Niu, Y. Li, J. Mol. Catal. A: Catal. 335 (2011) 71–81;
- (c) L.F. Liotta, G.A. Martin, G. Deganello, J. Catal. 164 (1996) 322–333.
- [28] M. Haruta, Gold Bull. 37 (2004) 27–36.
- [29] Q. Yao, C.L. Wang, H.W. Wang, H. Yan, J.L. Lu, J. Phys. Chem. C 120 (2016) 9174–9183.
- [30] T.M. Tran-Thuy, C.-C. Chen, S.D. Lin, ACS Catal. 7 (2017) 4304–4312.
- [31] M. Daté, M. Haruta, J. Catal. 201 (2001) 221–224.
- [32] H.H. Kung, M.C. Kung, C.K. Costello, J. Catal. 216 (2003) 425–432.
- [33] J. Saavedra, H.A. Doan, C.J. Pursell, L.C. Grabow, B.D. Chandler, Science 345 (2014) 1599–1602.